*Manuscript submitted to Polyhedron*

*as Research Paper*

# Cationic rhenium(I) complexes bearing a π-accepting pyridoannulated N-heterocyclic carbene ligand: synthesis, photophysical, electrochemical and theoretical investigation

*by*

Zakariae Asbai,[a,+] Anna Bonfiglio,[a,+] Pierluigi Mercandelli,[b] Federico Polo,[c] and Matteo Mauro,[a,*]

[a] *Institut de Physique et Chimie des Matériaux de Strasbourg, Université de Strasbourg-CNRS UMR 7504, 23 rue du Loess, BP 43, 67034 Strasbourg cedex 2, France. Fax: +33 (0)388107246; Tel: +33 (0)388107166; E-mail: mauro@unistra.fr*

[b] *Dipartimento di Chimica, Università degli Studi di Milano, via Camillo Golgi 19, 20133 Milano (Italy)*

[c] *Department of Molecular Sciences and Nanosystems, Ca' Foscari University of Venice, Via Torino 155, 30172 Venezia (Italy)*

[+] *these authors contributed equally to the work*

**Abstract**

A novel family of photoactive cationic *tris*-carbonyl rhenium complexes of general formula *fac*-[Re(CO)$_3$(pyipy)(L)]PF$_6$, where pyipy the 2-(pyridyl)-imidazo[1,5-*a*]pyridyl-3-ylidene ligand and L = pyridine (**3·PF$_6$**) or PPh$_3$ (**4·PF$_6$**), is herein presented. Compounds **3·PF$_6$** and **4·PF$_6$** are straightforwardly synthetized from the corresponding chloro-derivative *fac*-[ReCl(CO)$_3$(pyipy)] via halogen abstraction with silver(I) salt, followed by coordination of the neutral monodentate L ligand. The target complexes were characterized by $^1$H and $^{13}$C NMR as well as FT-IR spectroscopy and high-resolution mass spectrometry (HR-MS). In addition, X-ray diffractometric analysis was carried out by solving the single-crystal structure of compound **3·PF$_6$**. For both complexes, dilute samples in CH$_3$CN solution at room temperature display a structured photoluminescence profile in the red region that is ascribed to a long-lived excited state ($\tau$ = 19.3–30.0 μs in degassed condition) with mainly triplet ligand-centered ($^3$LC) character. This assignment is further corroborated by the minor hypsochromic shift of the emission profile observed for samples in 2-MeTHF at 77 K glassy matrix, in agreement with previous studies on the corresponding neutral counterparts. Electrochemical characterization by cyclic voltammetry (CV) shows two irreversible processes, one in the positive and one in the negative bias, which are associated to the metal-NHC moiety and the chelating NHC ligand, respectively. Finally, both electronic and optical features are further studied by means of computational investigation at density functional theory (DFT) and time-dependent DFT (TD-DFT) level of theory, which supports the attribution of the electronic transitions involved.

**Keywords:** carbonyl complexes, density functional theory, N-heterocyclic carbenes, phosphorescence, rhenium complexes

## 1. Introduction

The photophysics and photochemistry of metal carbonyl complexes have been matter of intense investigation due to their interesting optical and redox features,[1] since early works of Wrighton,[2] Rillema,[3] and Demas[4]. A particularly appealing class of photoactive complexes is represented by the family of mononuclear Re(I) *fac*-triscarbonyl derivatives bearing N-donor heteroaromatic ligands with accessible π* orbitals featuring π-accepting properties. The interest in such compounds was mainly driven by their appealing application in photocatalysis[5] (notably for $CO_2$ reduction and $H_2$ production), imaging probes in bio-medicine,[6] and emitters in organic light emitting diodes (OLEDs).[7]

In this framework, derivatives of general formula $[Re(N\hat{}N)(CO)_3L]^{n+}$, where N^N is a bidentate N-heterocyclic ligand such as 2,2'-bipyridine, 1,10-phenanthroline and related scaffolds, and L is either an anionic monodentate ancillary ligand (L = halogen, cyanide, alkoxy, alkynyl, *etc.*; $n$ = 0) or a neutral ligand such as pyridines, phosphines, isonitriles (with $n$ = 1), are the most investigated ones by far. Several studies have shown that these compounds display broad and featureless photoluminescence in the green-to-red portion of the electromagnetic spectrum with excited state lifetime ranging from hundreds of nanoseconds to a few microseconds time scale. The nature of the emissive excited state may vary from purely triplet metal-to-ligand charge transfer ($^3$MLCT) to ligand-to-ligand charge transfer ($^3$LLCT) and up to (sizable) triplet ligand-centered ($^3$LC) character depending on the nature and electronic properties of both the N^N and the ancillary ligand, with often a certain degree of mixing between the two states.[2,3] Hence, a metal-ligand-to-ligand character is more often associated to the emissive triplet manifold ($^3$MLLCT). Photoluminescence quantum yield (PLQY) values largely varies as well, being cationic rhenium(I) complexes typically more efficient than neutral counterparts with values almost one order of magnitude higher for the former.[4] Furthermore, neutral dinuclear species of general formula $[Re_2(\mu\text{-}X)_2(CO)_6(\mu\text{-diaz})]$, where

X = halogen and diaz = 1,2-diazine type of ligands, have shown superior properties and efficient electroluminescence, as reported by some of us.[8]

Surprisingly, the vast majority of the phosphorescent derivatives containing the $Re(CO)_3$ unit investigated so far features poly-pyridine type of ligands. On the other hand, limited attention has been devoted to investigate alternative ligands, in particular those containing stronger σ-donating moieties, such as N-heterocyclic carbenes (NHCs). This is in spite of the fact that NHC are outstanding ligands in organometallic chemistry,[9] and have demonstrated to play pivotal role in the preparation of efficient emitters with other transition metals,[10] including Ir(III),[11] Pt(II),[12] Au(I),[13] and Cu(I)[14].

In this respect, Che and co-workers firstly described a series of $[Re(N\text{^}N)(CO)_3(NHC)]X$ complexes featuring an NHC as the ancillary ligand.[15] It is only in 2011 that Massi and co-workers[16] described the first examples of photoactive Re(I) *tris*-carbonyl complexes bearing an NHC as the chromophoric ligand, namely $[ReX(CO)_3(C\text{^}N)]$ with X = $Cl^-$, $Br^-$ and C^N = 3-butyl-1-(2'-pyridyl)benzimidazolin-2-ylidene NHC ligand. The complexes displayed $^3$MLCT emission in the green-yellow region with PLQY ≤1%. In related derivatives, energetic stabilization of the π* orbitals located onto the heteroaromatic ligand, achieved through extension of the π-system and/or introduction of additional heteroatoms,[17] gave rise to a bathochromic shift of the $^3$MLCT emission wavelength, as expected. This shift was accompanied in some cases by a prolongation of the excited state lifetime up to τ = 1.07 μs and an increase of the PLQY, with values falling in the range 0.1–13%. On the other hand, employment of the 3-(pyrid-2-yl)dimethylthiazol-2-ylidene as the NHC ligand gave a yellow phosphorescent complex displaying PLQY = 4% and τ = 399 ns.[18] Concomitantly, Zheng and co-workers described related derivatives with either π-conjugated or methylene-bridged C^N ligands containing pyridyl-benzimidazolin-2-ylidene, pyridyl-imidazolin-2-ylidene and 2-pyridyl-1,2,4-triazoline-5-ylidene NHC scaffolds.[19] They found that the rupture of the π–conjugation between the π-accepting pyridyl group and the carbene moiety is detrimental for the

emission properties of the final complex. Whereas, conjugated counterparts display photophysical properties that agrees with that earlier reported by Massi.[16-18]

Prompted by our interest in the photophysics of novel rhenium(I) carbonyl compounds and encouraged by our previous results,[20] we aim herein at investigating the effect of neutral *vs.* cationic nature of the complexes onto both optical and redox properties in this family of *tris*-carbonyl rhenium(I) complexes bearing the pyridyl pyridoannelated NHC ligand, namely [pyipy]$PF_6$. The variation of the overall charge of the complex is known to have profound effects on the photophysical properties of diimine-based counterparts.[2-4] However, to the best of our knowledge, it has been overlooked for Re-NHC complexes. Herein, the synthesis, chemical, electrochemical and photophysical characterization of a series of $[Re(CO)_3(pyipy)(L)]PF_6$, where L = pyridine, $PPh_3$, is presented along with the experimental data, which have been thoroughly rationalized also by means of computational approaches.

## 2. Synthesis and X-ray characterization

The synthetic pathway employed for the synthesis of the target cationic complexes **3·PF$_6$** and **4·PF$_6$** is displayed in Scheme 1. The *tris*-carbonyl rhenium halo-complex **1**–**2** from [pyipy]$PF_6$ and $[ReX(CO)_5]$ (X = Cl, Br), previously described by us elsewhere,[20] represent the starting material to synthesize the novel Re complexes. De-halogenation procedure is carried out by treatment with an Ag(I) source and metathesis with a $PF_6^-$ salt in a coordinating solvent, such as $CH_3CN$, yielding the intermediate *solvo*-complex $[Re(CO)_3(pyipy)(CH_3CN)]PF_6$. This latter is readily reacted with a monodentate ligand in THF to give the desired cationic complex **3·PF$_6$** and **4·PF$_6$**, where L is pyridine and triphenylphosphine, respectively, as pale-yellow air-stable solids. The target complexes were fully characterized by means of $^1H$ and $^{13}C\{^1H\}$ NMR with spectra matching the predicted set of signals. Elemental analysis and high-resolution electron spray ionization mass spectrometry (HR-

ESI-MS) techniques further confirmed the nature and the purity of the obtained compounds. The corresponding spectra are displayed in Figure S1–S6 of the Supporting Information.

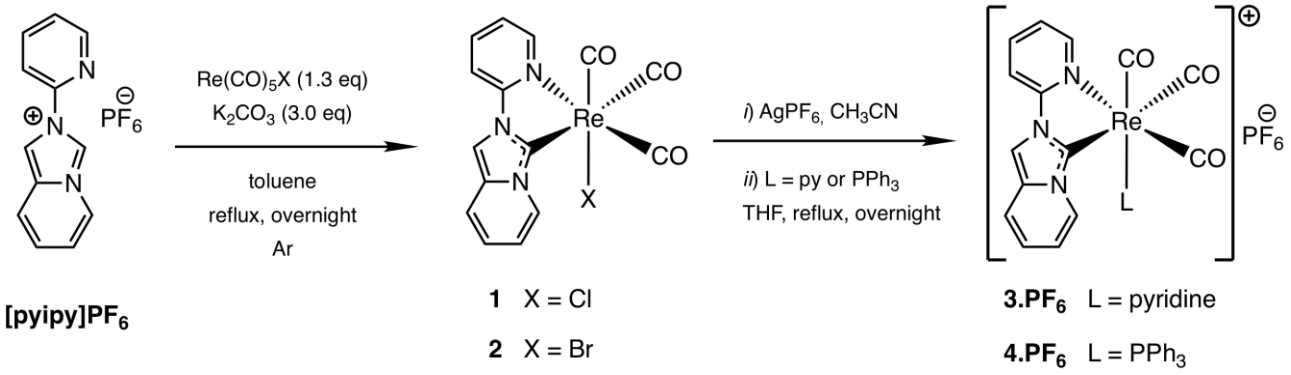


**Scheme 1.** Schematic synthetic pathway used for the preparation of the cationic complexes **3·PF6** and **4·PF6**.

Suitable crystals of this latter were obtained by slow diffusion of *n*-hexane into a THF solution of the complex, which allowed to establish atom connectivity and geometrical parameters by solving the single crystal X-ray structure of derivative **3·PF6**. The corresponding ORTEP diagram is displayed in Figure 1 and the crystallographic refinement parameters and metrics data are listed in Table S1–S2 of the Supporting Information. The X-ray structure shows a distorted octahedral arrangement of the coordinated ligands around the metal center, with the three carbonyls adopting a mutual *facial* arrangement, as expected. Among the three different Re–CO bond, the one lying in *trans* to the carbene moiety displays the longer Re–C bond distance, reflecting the larger *trans* influence exerted by the strong σ-donating moiety. A pyridine ligand completes the coordination sphere occupying remaining position.

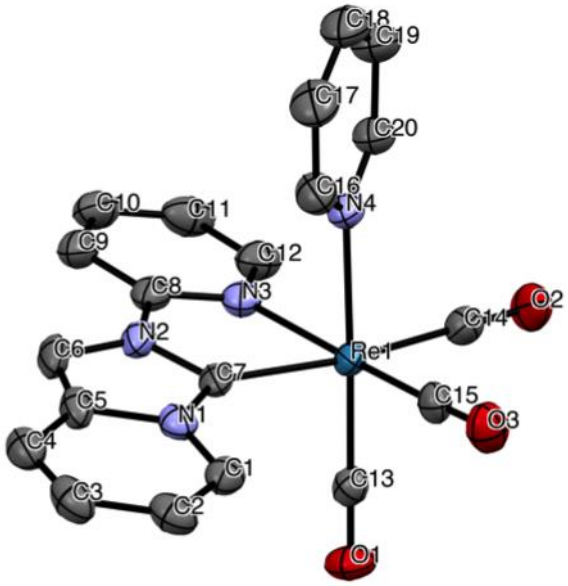


**Figure 1.** ORTEP diagram of compound **3·PF$_6$·THF** with thermal ellipsoids shown at 50% probability level obtained by single-crystal X-ray diffractometric analysis. Hydrogen atoms, $PF_6^-$ anion and THF solvent molecule are omitted for clarity. Selected bond lengths (Å): Re–C(7) = 2.137(5) Å; Re–C(13) = 1.920(5) Å; Re–C(14) = 1.967(6) Å, Re–C(15) = 1.917(5) Å, Re–N(3) = 2.221(4) Å; Re–N(4) = 2.216(4) Å.

### 3. Electrochemistry

The electrochemical behaviour of **3·PF$_6$** and **4·PF$_6$** was assessed by cyclic voltammetry (CV) in *N*,*N*-dimethylformamide (DMF)/0.1 M tetra-*n*-butylammonium perchlorate (TBAP) and showed the same pattern previously observed for neutral parental complexes **1** and **2**.[20] In fact, as displayed in Figure 2, compound **3·PF$_6$** and **4·PF$_6$** showed an irreversible oxidation process ($O_1$) in the positive bias, which is commonly observed for Re carbonyl complexes, at $E_{O1}$ = +1.340 V and +1.391 V *vs* SCE, respectively. In the negative bias, one main irreversible reduction process ($R_1$) occurs at $E_{R1}$ = –1.285 V and –1.479 V *vs* SCE for **3·PF$_6$** and **4 PF$_6$**, respectively. To better appreciate the redox processes, $O_1$ and $R_1$ were recorded separately and the voltammograms are shown in Figure 2. The electrochemical data are summarized in Table 1. The redox potential values for both $O_1$ and $R_1$

processes of **3·PF$_6$** and **4·PF$_6$** are shifted anodically, compared to **1** and **2**,[20] due to the overall cationic character of rhenium(I) complex upon substitution of chloride with the neutral pyridine or triphenylphosphine ancillary ligand. In fact, $O_1$ and $R_1$ are related to the oxidation of the metal-NHC moiety and to the reduction of the chelating NHC ligand, respectively. With respect to **3·PF$_6$**, $O_1$ occurs at more positive potentials (*ca.* 200 mV) than that of **1** and **2**, whereas the electrochemical band gap is only slightly affected (*ca.* 0.1 eV), as reported in Table 1. Instead, with respect to **4·PF$_6$**, $O_1$ occurs at even more positive potential compared to **3·PF$_6$** (*ca.* 50 mV), whereas $R_1$ is sizeably shifted cathodically (*ca.* 200 mV), owing to the triphenylphosphine ligand. The latter one led the bandgap to widen to 2.85 eV. Overall, the electrochemical data are in qualitative agreement with the widening of the optical bandgap observed in the UV-visible spectrum going from the neutral complex **2** to the cationic derivatives **3·PF$_6$** and **4·PF$_6$**, as demonstrated by the hypsochromic shift of the onset of the $^1$MLCT band recorded for these latter (see photophysics section).

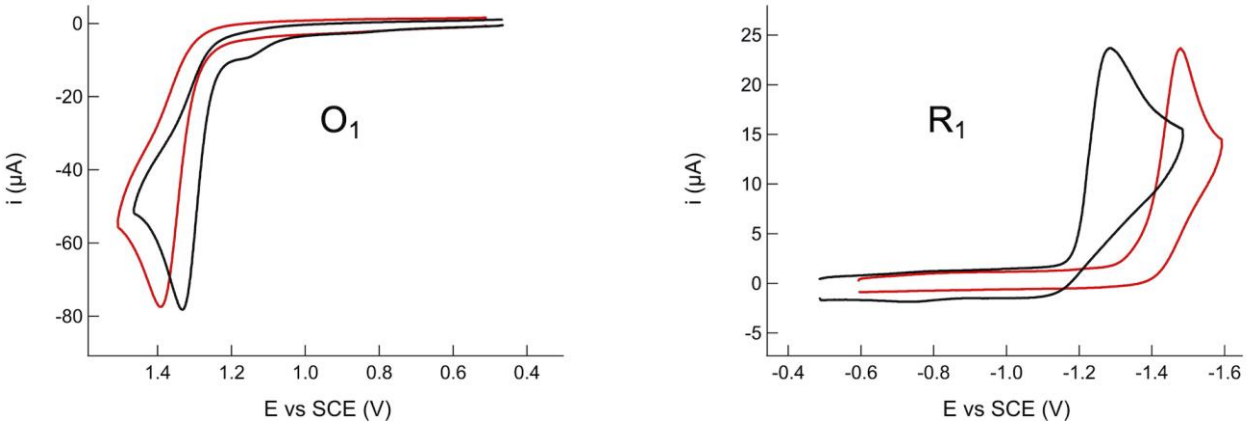


**Figure 2.** CVs recorded showing $O_1$ and $R_1$ redox processes for 1 mM of compounds **3·PF$_6$** (black) and **4·PF$_6$** (red) in DMF/0.1 M TBAP. Scan rate: 0.2 V s$^{-1}$.

**Table 1.** Electrochemical data for compound **3·PF$_6$** and **4·PF6** obtained by cyclic voltammetry (CV) carried out in DMF and 0.1 M TBAP as the supporting electrolyte. Data for compound **1**–**2** and the chelating ligand **[pyipy]PF$_6$** are also reported from Ref. 20 for comparison.

| Cmpd | $E_{p\|O1}$ [V] [a] | $\Delta E_{p/2\|O1}$ [mV] [b] | $E_{p\|R1}$ [V] [a] | $\Delta E_{p2\|R1}$ [mV] [b] | *Gap* [eV] | Ref. |
|---|---|---|---|---|---|---|
| **1** | +1.151 | 46 | -1.586 | 54 | 2.737 | [20] |
| **2** | +1.177 | 55 | -1.543 | 60 | 2.720 | [20] |
| **3·PF$_6$** | +1.340 | 51 | -1.285 | 54 | 2.625 | Present work |
| **4·PF$_6$** | +1.391 | 54 | -1.479 | 54 | 2.870 | Present work |
| **[pyipy]PF$_6$** | | | -1.507 | 88 | | [20] |

[a] Potential values are referred to SCE at the scan rate of 0.1 Vs$^{-1}$. [b] $\Delta E_{p/2}$ is defined as $E_p$-$E_{p/2}$, where $E_{p/2}$ is the potential value when the current $i$ is at half its peak value, $i_p$, for the processes under investigation ($O_1$ or $R_1$, respectively).

The effect of the scan rate was investigated over the range 50–500 mV s$^{-1}$, and the peak current was found to depend linearly on the square root of scan rate (data not shown) thus witnessing that the heterogeneous electron transfer process is diffusion-controlled. On the other hand, $E_p$-$E_{p/2}$ varied in the range of 45–60 mV regardless of the scan rate, while peak potentials shifted towards more positive potentials (by *ca.* 20 mV) for $O_1$ and more negative potentials (by *ca.* 40 mV) for $R_1$. These data are in agreement with the occurrence of a diffusion-controlled heterogeneous electron transfer reaction, followed by a very fast chemical reaction (EC process).[21]

## 4. Photophysics

The photophysical properties of complexes **3·PF$_6$** and **4·PF$_6$** were investigated at concentration of $2\times10^{-5}$ M in both air-equilibrated and degassed acetonitrile solution at room temperature as well as at 77 K in 2-MeTHF glassy matrix. The electronic absorption and the normalized emission spectra are displayed in Figure 3 and the corresponding photophysical data are listed in Table 2. In the UV range, an intense absorption band in observed with $\lambda_{abs,max}$ = 237 nm ($\varepsilon = 2.61\times10^4$ M$^{-1}$ cm$^{-1}$) and $\lambda_{abs,max}$ = 231 nm ($\varepsilon = 4.22\times10^4$ M$^{-1}$ cm$^{-1}$) for compound **3·PF$_6$** and **4·PF$_6$**, respectively. This band can be mainly ascribed to ligand-centered transitions localized onto the coordinated NHC-ligand in

agreement with computational investigation (*vide infra*) as well as previously reported investigation on the neutral congeners.[20] The additional contribution of the π-π* transitions involving the phenyl rings of the $PPh_3$ ligand in compounds **4·PF$_6$** accounts for the increased molar extinction coefficient observed for this complex. At lower energy, the absorption band observed in the region at $\lambda_{abs}$ *ca.* 400 nm is ascribed to an electronic transition with $^1$MLCT character, namely d(Re)$\pi_{NHC} \rightarrow \pi^*_{py}$, admixed with intraligand charge-transfer ($^1$ILCT) involving the cyclometalating ligand with $\pi_{NHC} \rightarrow \pi^*_{py}$ nature, where NHC is the benzannulated NHC moiety and py is the pyridyl ring. Further details concerning the frontier orbitals involvement in the electronic transitions are provided in the theoretical section.

Upon irradiation at the $^1$MLCT band, complexes **3·PF$_6$** and **4·PF$_6$** show similar photophysical properties. The photoluminescence spectrum of both samples in degassed $CH_3CN$ show a structured emission with maxima at $\lambda_{em}$= 602 and 606, 660 and 725 nm at room temperature that are Stokes shifted by *ca.* 6500 and 6650 cm$^{-1}$ for **3·PF$_6$** and **4·PF$_6$**, respectively. The photoluminescence profile is independent of the presence of dioxygen molecules and excitation wavelength. Furthermore, similar vibronic progression is observed with fundamental spacing of *ca.*1350 cm$^{-1}$ that is attributable to intraligand modes of the cyclometalatated pyipy scaffold. Upon removing dioxygen, increase of the photoluminescence quantum yield (PLQY) values (from 0.14% to 0.72%) as well as prolongation of the excited-state lifetime (from τ = 204 ns to 19.3 μs) is observed for compound **3·PF$_6$**. Likewise, PLQY and lifetime increase from 0.04% to 1.60% and τ = 209 ns to 30.0 μs, respectively, for derivative **4·PF$_6$**. Going from room temperature to 77 K glassy matrix, the photoluminescence spectra display a minor hypsochromic shift and band profile becomes even more structured. Overall, these findings along with the small $k_r$ values, being in the range 3.8–5.3×10$^3$ s$^{-1}$, are indicative for an excited state with largely triplet ligand-centered ($^3$LC) character, in agreement with related complexes **1**–**2** reported previously.[20]

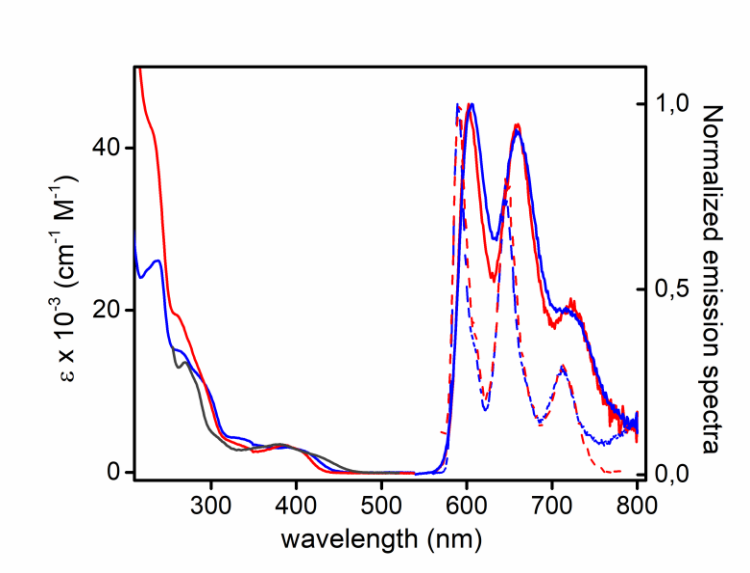


**Figure 3.** Electronic absorption and photoluminescence spectra of compound **3·PF$_6$** (blue traces) and **4·PF$_6$** (red traces) and in degassed $CH_3CN$ solution at a concentration of $2\times10^{-5}$ M at room temperature (solid line) and 77 K (dashed line). The UV-visible spectrum of the parental complex **1** in $CH_2Cl_2$ (black trace) is displayed as well for comparison. Emission spectra at 298 K were recorded upon excitation at $\lambda_{exc}$ = 420 and 440 nm for compound **3·PF$_6$** and **4·PF$_6$**, respectively. Emission spectra at 77 K were recorded upon excitation at $\lambda_{exc}$ = 400 and 420 nm for compound **3·PF$_6$** and **4·PF$_6$**, respectively.

## 5. Computational investigation

To support the interpretation of the photophysical and electrochemical data, the electronic structures of the cationic complexes **3**$^+$ and **4**$^+$ and their absorption and emission spectra were computed in acetonitrile employing density functional and time-dependent density functional theory along with the polarizable continuum model (PCM) of solvation (see experimental section). Molecular orbital plots and electron density difference maps (EDDM) computed for compound **3**$^+$ are displayed in Figure 4 and Figure 5, respectively; whereas, tables of calculated electronic transition properties are

available as Supporting Information in Table S3. For compound $\mathbf{4}^{+}$, corresponding data are available in Figure S9 and Table S4.

According to the calculations, in $\mathbf{3}^{+}$ the rhenium d orbitals mainly contribute to the four highest occupied molecular orbitals, close-lying in energy. The HOMO and HOMO–3 are the two combinations (anti-phase and in-phase, respectively) of one of the d orbitals and the highest lying π orbital of the heterocyclic carbene moiety. On the contrary, the HOMO–1 and HOMO–2 do not show contributions from the organic ligand. In these four orbitals no contribution from the pyridine ancillary ligand is present. Lying at lower energy, HOMO–4 is a ligand π orbital extended over both the pyridyl and the heterocyclic carbene rings. The lowest unoccupied molecular orbital is a π* orbital delocalized all over the pyridylcarbene ligand. In addition, the LUMO+1 shows a substantial contribution from the lowest π* orbital of the pyridine ancillary ligand.

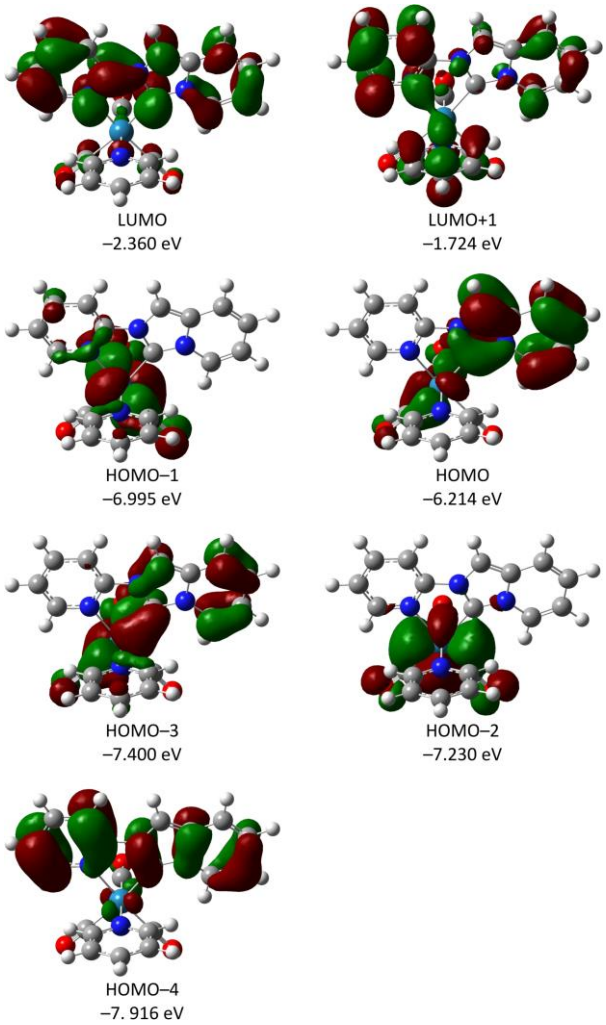

**Figure 4.** Isodensity surface plots and energies computed for some relevant molecular orbitals of *fac*-[Re(pyipy)(CO)$_3$(py)]$^+$ (**3**$^+$).

The bands at lower energies in the absorption spectrum of complex **1** can be assigned to the superposition of two electronic transitions, $S_0 \rightarrow S_1$ and $S_0 \rightarrow S_2$ at 403 and 337 nm, corresponding mainly to the HOMO→LUMO and HOMO–1→LUMO monoelectronic excitations, respectively. According to the nature of the orbitals involved, and looking at the corresponding electron density difference maps (EDDM), both transitions imply a significant MLCT character. The lower-energy transition, however, shows also a noticeable intraligand (IL) character. In particular, it displays a net charge transfer from the heterocyclic carbene ring to the pyridyl moiety.

Two intense electronic transitions, $S_0 \rightarrow S_{19}$ and $S_0 \rightarrow S_{29}$ at 255 and 229 nm, dominate the region at higher energy and correspond to the two peaks observed experimentally at 265 and 237 nm. They correspond to some complex admixtures of many monoelectronic excitations, mainly HOMO–3→LUMO+1, HOMO–4→LUMO+1 and HOMO→LUMO+10 (among many others). None of these transitions can be described as strictly LC only, since the redistribution of the electron density within the pyridylcarbene ligand is accompanied also by a charge transfer between the carbene and the ancillary ligand and by some redistribution of the electrons within the set of rhenium d orbitals. The complex nature of these transitions can also be appreciated from the corresponding electron density difference maps reported in the Supporting Information.

Geometry optimization of the lowest-lying triplet for cation **3**$^+$ leads to the individuation of a species analogous to that previously found for the neutral complexes **1** and **2**.[20] In particular, with respect to the ground state, the triplet $T_1$ shows an altered alternation of short and long bond lengths within the heterocyclic carbene moiety, leaving the rest of the molecule almost unaltered, in agreement with the LC nature of the $T_1 \rightarrow S_0$ transition. The same conclusion is reached when considering the corresponding EDDM, in which only a limited contribution of a rhenium d orbital

can be detected, while the orbitals of the pyridine ancillary ligand are not involved at all. The electron density difference map computed for the cationic species $\mathbf{3}^+$ shows an enhanced LC character of the emission with respect to the neutral species **1**, in agreement with an increased contribution of the π orbital of the carbene ligand to the HOMO (69% and 52% in $\mathbf{3}^+$ and **1**, respectively).

Both vertical and adiabatic energies have been computed for the $T_1 \rightarrow S_0$ transition (see Figure 5). As expected, due to the substantial difference between the triplet and the ground-state geometry, vertical and adiabatic values are quite different (0.376 eV). The adiabatic energy computed for the $T_1 \rightarrow S_0$ transition slightly underestimate the experimental value (624 vs 606 nm, corresponding to a difference of –0.058 eV or –464 $cm^{-1}$). The vibrationally resolved emission spectra computed within the framework of the Franck-Condon principle reproduces reasonably well the observed additional maxima (673 and 752 nm vs 660 and 725 nm). As expected for a LC transition, the normal mode primarily contributing to the vibronic structure of the band is an IL one, and, in particular, an in-plane ring deformation ($\nu_{97}$, see Figure S10 – S11 of the Supporting Information).

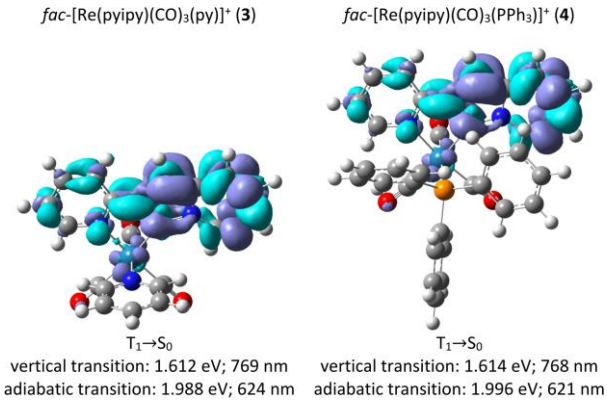


**Figure 5.** Electronic density difference maps computed (at the optimized geometry of the corresponding triplet) for the vertical transition $T_1 \rightarrow S_0$ of *fac*-$[Re(pyipy)(CO)_3(py)]^+$ (**3**) and *fac*-$[Re(pyipy)(CO)_3(PPh_3)]^+$ ($\mathbf{4}^+$). Energy computed for the corresponding adiabatic transition is also reported. Cyan and violet indicates a decrease and increase in electron density, respectively.

Results for the triphenylphosphine derivative $\mathbf{4}^{+}$ are analogous to the ones already described for the pyridine counterpart $\mathbf{3}^{+}$. However, in **4** the set of π orbitals of the phenyl rings of the phosphine ligand partially overlaps in energy with some of the rhenium d orbitals and with the π orbitals of the carbene ligand. The bonding and antibonding π orbital of the phenyl groups do not contribute to the lowest energy bands in the absorption spectra. Triphenylphosphine π–π* monoelectronic excitations, however, leads to an even more complex nature of the bands at higher energy. On the other hand, the computed emission energy remains almost unaltered on going from $\mathbf{3}^{+}$ to $\mathbf{4}^{+}$, in agreement with the nature of the $T_1 \rightarrow S_0$ transition that does not show contributions from the orbitals of the ancillary ligand.

**Table 2.** Photophysical data for complexes **3·PF$_6$** and **4·PF$_6$** recorded in air-equilibrated and degassed $CH_3CN$ solution at room temperature and 77 K 2-MeTHF glassy matrix.

| **Cmpd** | **$\lambda_{max,abs}$ ($\varepsilon$)** [nm, ($10^3$ $M^{-1}$ $cm^{-1}$)] | **$\lambda_{em}$** [nm] | | **PLQY** (%) | | **$\tau_{obs}$** | | **$k_r$** [$10^3$ $s^{-1}$] | **$k_{nr}$** [$10^4$ $s^{-1}$] | **$\lambda_{em}$** [nm] |
|---|---|---|---|---|---|---|---|---|---|---|
| | | *air equilibrated* | *degassed* | *air equilibrated* | *degassed* | *air equilibrated* | *degassed* | | | *77 K* |
| **3·PF$_6$** | 405 (2.77), 339 (4.07), 265 (14.88), 237 (26.09) | 606, 660, 725 | 606, 660, 725 | 0.14 | 0.72 | 204 ns | 19.3 | 3.79 | 5.23 | 592, 647, 710 |
| **4·PF$_6$** | 394 (3.00), 329 (3.53), 261 (19.29), 231 (42.15) | 602, 660, 725 | 602, 660, 725 | 0.04 | 1.60 | 209 ns | 30.0 µs | 5.33 | 3.28 | 592,647, 710 |

## 6. Experimental section

### *General considerations*

[$ReCl(CO)_5$] was purchased from Acros. The synthesis of complex **1** was carried out following a procedure reported elsewhere by us.[20] All procedures involving rhenium complexes were carried out under an argon atmosphere using standard Schlenk techniques. Silica gel for column chromatography was purchased from Sigma-Aldrich. Nuclear magnetic resonance spectra were recorded using a Bruker Avance III HD 500 spectrometer equipped with a $N_2$ cryo-probe CPPBBO Prodigy at 298 K. $^1H$ and $^{13}C\{^1H\}$ NMR spectra were calibrated to residual solvent signals. Infrared spectra were recorded using a Fourier-transformed attenuated total reflectance infrared (FT-ATR-IR) spectrometer from PerkinElmer. Elemental analyses were obtained at the AMS Fédération de Chimie Le Bel, University of Strasbourg on a Flash 2000 ThermoFischer Scientific apparatus. HR-ESI-MS spectra were recorded on a MicroToF Bruker equipped with an electrospray ionization source.

### *Synthesis*

**3·$PF_6$**. Complex **1** (100 mg, 0.20 mmol) and $AgPF_6$ (87 mg, 0.26 mmol) were dissolved in 10 mL of $CH_3CN$ and refluxed in the dark for 18 h. The yellow solution was filtered on Celite to remove AgCl and then the solvent was evaporated. The crude was dissolved in 5 mL of dry THF and pyridine (16 mg, 0.20 mmol) was added under an argon atmosphere. The mixture refluxed for 2 hours. After cooling down the solution, THF was evaporated and the crude was purified on chromatographic column on $SiO_2$ using $CH_2Cl_2$ as eluent mixture. An air-stable yellow solid was obtained. Yield 25% (38 mg, 0.05 mmol). $^1H$ NMR (500 MHz, 298 K, $CD_2Cl_2$) δ: 9.07 (ddd, *J* = 5.6, 1.5, 0.6 Hz, 1H), 8.49 (dd, *J* = 7.3, 1.0 Hz, 1H), 8.39–8.34 (m, 2H), 8.24 (m, 2H), 8.19 (d, *J* = 8.3 Hz, 1H), 7.83 (tt, *J* = 7.7, 1.5 Hz, 1H), 7.69 (ddd, *J* = 7.6, 5.6, 1.1 Hz, 1H), 7.64 (dt, *J* = 9.4, 1.0 Hz, 1H), 7.33–7.29 (m, 2H), 7.14 (dd, *J* = 9.4, 6.5 Hz, 1H), 7.05–7.01 (m, 1H). $^{13}C\{^1H\}$ NMR (126 MHz, 298 K, $CD_2Cl_2$) δ: 206.5, 196.9, 189.4, 180.5, 153.5, 143.7, 139.2, 133.2, 126.9, 126.2, 124.9, 119.1, 117.5, 114.8, 108.6,

53.5, 30.6. Elemental analysis for $C_{20}H_{14}F_6N_4O_3PRe$ Calcd C 34.84 H 2.05 N 8.13, found C 34.12 H 2.08 N 7.87.

**4·PF$_6$**. For complex **4·PF$_6$**, a modified version of that previously reported for the synthesis of related $[Re(CO)_3(N\text{^}N)(PPh_3)]PF_6$ derivatives was employed.[22] Complex **1** (100 mg, 0.2 mmol) and AgOTf (66 mg, 0.26 mmol) were dissolved in 10 mL of $CH_3CN$ and heated at 85 °C under the dark for 12 h. The yellow solution was filtered over Celite, then concentrated until 2 mL. A volume of 5 mL of saturated aqueous $KPF_6$ was added dropwise to the solution. The suspension was kept stirring for 1 hour, then dried on the rotary evaporator to eliminate $CH_3CN$. The precipitate was filtered, washed with ethanol and diethyl ether and air-dried. The obtained solid was dissolved in 10 mL of dry THF and $PPh_3$ (1.0 g, 4 mmol) was added. The resulting mixture heated at 77 °C for 12 h under argon. The solvent was evaporated and the crude was purified by chromatographic column on $Al_2O_3$ using hexane/DCM (20:80) as eluent mixture to obtain a green oil. The oil was dissolved in 1 mL of DCM and diethyl ether was added dropwise under stirring until a solid precipitate. The solution was carefully removed with a syringe and the solid dried. An air-stable pale-greenish solid was collected. Yield 25% (50 mg, 0.05 mmol). $^1$H NMR (500 MHz, $CD_2Cl_2$) δ: 8.46–8.43 (m, 1H), 8.29 (s, 1H), 8.18–8.13 (m, 1H), 8.00 (d, *J* = 8.3 Hz, 1H), 7.86 (dd, *J* = 7.4, 1.0 Hz, 1H), 7.52 (d, *J* = 9.4 Hz, 1H), 7.38 (td, *J* = 7.4, 1.8 Hz, 3H), 7.28 (td, *J* = 7.7, 2.5 Hz, 6H), 7.22–7.18 (m, 1H), 7.16–7.10 (m, 6H), 7.01 (dd, *J* = 9.4, 6.5 Hz, 1H), 6.76 – 6.72 (m, 1H). $^{13}$C{$^1$H} NMR (126 MHz, $CD_2Cl_2$) δ: 206.9, 206.4, 195.95, 195.9, 195.6, 195.5, 185.7, 185.2, 175.4, 175.3, 153.7, 152.5, 142.5, 133.4, 132.5, 132.4, 131.0, 130.3, 130.0, 129.0, 129.0, 126.6, 125.1, 124.5, 119.0, 116.5, 114.4, 108.6. Elemental analysis for $C_{33}H_{24}F_6N_3O_3P_2Re$ Calcd C 45.42 H 2.77 N 4.81, found C 44.44 H 3.05 N 4.33.

***X-ray diffractometric analysis***

The crystals were placed in oil, and a single crystal was selected, mounted on a glass fibre and placed in a low-temperature $N_2$ stream. X-ray diffraction data collection was carried out on a Bruker PHOTON III DUO CPAD diffractometer equipped with an Oxford Cryosystem liquid $N_2$ device,

using Mo-Kα radiation (λ = 0.71073 Å). The crystal-detector distance was 37 mm. The cell parameters were determined (APEX3 software)[23] from reflections taken from 1 set of 180 frames at one second exposure time. The structure was solved using the program SHELXT-2014.[24] The refinement and all further calculations were carried out using SHELXL-2014.[25] The H-atoms were included in calculated positions and treated as riding atoms using SHELXL default parameters. The non-H atoms were refined anisotropically, using weighted full-matrix least-squares on $F^2$. A semi-empirical absorption correction was applied using SADABS in APEX3.[23]

***Photophysical characterization***

*Instrument details.* Absorption spectra were measured on a Varian Cary 100 double-beam UV–VIS spectrophotometer and baseline corrected. Steady-state emission spectra were recorded on a Horiba Jobin–Yvon IBH FL-322 Fluorolog 3 spectrometer equipped with a 450 W xenon arc lamp, doublegrating excitation, and emission monochromators (2.1 nm $mm^{-1}$ of dispersion; 1200 grooves $mm^{-1}$) and a Hamamatsu R13456 red sensitive Peltier-cooled PMT detector. Emission and excitation spectra were corrected for source intensity (lamp and grating) and emission spectral response (detector and grating) by standard correction curves. Time-resolved measurements were performed using either the time-correlated single-photon counting (TCSPC) or the Multi-Channel Scaling (MCS) electronics option of the TimeHarp 260 board installed on a PicoQuant FluoTime 300 fluorimeter (PicoQuant GmbH, Germany), equipped with a PDL 820 laser pulse driver. A pulsed laser diode LDH-P-C-375 ($\lambda_{exc}$= 375 nm, pulse full width at half maximum FWHM <50 ps, repetition rate 200 kHz–40 MHz) was used to excite the sample and mounted directly on the sample chamber at 90°. The photons were collected by a PMA Hybrid-07 single photon counting detector. The data were acquired by using the commercially available software EasyTau II (PicoQuant GmbH, Germany), while data analysis was performed using the built-in software FluoFit (PicoQuant GmbH, Germany). Data fitting was performed by employing the maximum likelihood estimation (MLE) methods and the quality of the fit was assessed by inspection of the reduced $\chi^2$ function and of the

weighted residuals. Luminescence quantum yields were measured in optically dilute solutions (optical density <0.1 at the excitation wavelength) and compared to reference emitter by following the method of Demas and Crosby.[26] The $Ru(bpy)_3Cl_2$ complex in air-equilibrated water solution at room temperature was used as reference (PLQY = 0.04).[27] All the solvents were spectrophotometric grade. Dearated samples were prepared by the freeze–pump–thaw technique by using a home-made quartz cuvette equipped with a Rotaflo stopcock.

***Electrochemistry***

Anhydrous *N*,*N*-dimethylformamide (DMF, Sigma-Aldrich, 99.8%) and tetra-n-butylammonium perchlorate (TBAP, Fluka, 99%) were used as received. The working electrode was a glassy-carbon disk electrode (2 mm diameter, Princeton Applied Research GO224). The electrode was polished as already described elsewhere.[28] Before experiments, the electrode was further polished with a 0.05 μm polycrystalline diamond suspension (Buehler, MetaDI) and electrochemically activated in the background solution by means of several voltammetric cycles at 0.5 V $s^{-1}$ between the anodic and the cathodic solvent/electrolyte discharges, until the expected quality features were attained.[29] A platinum wire served as the counter electrode and a silver wire, separated from the main electrolytic compartment by a Vycor® frit, was used as a quasi-reference electrode. At the end of each experiment, its potential was calibrated against the ferricenium/ferrocene couple, used as an internal redox standard. In DMF/0.1 M TBAP, ferricenium/ ferrocene has a formal potential of 0.464 V against the KCl saturated calomel electrode (SCE),[28] which allows to reference all the potentials against SCE. The cyclic voltammetry (CV) experiments were carried out in DMF/0.1 M TBAP under an Ar atmosphere, using a 1 mM concentration for the electroactive compound. A CHI 760D Electrochemical Workstation (CH Instruments) was used. For the CV experiments, we employed the feedback correction to minimize the ohmic drop between the working and the reference electrodes.

***Computational details***

Ground state and low-lying triplet geometries were optimized by means of density functional calculations. The parameter-free hybrid functional PBE0[30] was employed along with the standard valence double-ζ polarized basis set 6-31G(d,p) for C, H, N, O and P. For Re the Stuttgart–Dresden effective core potentials were employed along with the corresponding valence triple- ζ basis set. All the calculations were done in the presence of acetonitrile, used in the photophysical characterizations, described by a polarizable continuum model (PCM)[31]. Optimization of the ground state geometry in dimethylformamide, used in the electrochemical characterization, gives almost indistinguishable results (difference in bond distances lower than 0.0001 Å and differences in orbital energies lower than 0.003 eV). Only data computed in acetonitrile are described. The nature of all the stationary points was checked by computing vibrational frequencies and all the geometries were found to be true minima. In order to simulate the absorption electronic spectrum down to about 220 nm the lowest 40 (or 60) singlet excitation energies were computed for $\mathbf{3}^{+}$ (or $\mathbf{4}^{+}$) by means of time-dependent density functional calculations. The vibrationally-resolved emission spectra were simulated in the framework of the Franck-Condon principle,[32] shifting the 0–0 energy to its observed value. All the calculations were done with Gaussian 16 software package.[33]

## 7. Conclusion

Two novel cationic *tris*-carbonyl rhenium complexes bearing the pyridoannulated NHC ligand pyipy is reported. For one of the derivatives, namely compound **3·PF$_6$**, atom connectivity was unambiguously ascertained by solving the single-crystal X-ray structure. Both compounds display long-lived emission with structured profile in the red portion of the electromagnetic spectrum. The photoluminescence is attributed to an exited state with mainly $^3$LC character as jointly supported by photophysical characterization and TD-DFT analysis. While the charged nature of the complex seems to do not affect the photoluminescence properties to a large extent, modulation of the redox properties was clearly achieved instead. Indeed, oxidation and reduction potential shifted anodically and

cathodically, respectively, when compared to the parental neutral congeners. Overall, these features make the described class of photoactive Re-NHC complexes suitable candidates for potential application in photocatalysis under visible light irradiation.

## 8. Conflicts of interest

There are no conflicts to declare.

## Appendix A. Supplementary data.

CCDC 2036080 contains the supplementary crystallographic data for **3·PF$_6$·THF**. These data can be obtained free of charge via http://www.ccdc.cam.ac.uk/conts/retrieving.html, or from the Cambridge Crystallographic Data Centre, 12 Union Road, Cambridge CB2 1EZ, UK; fax: (+44) 1223-336-033; or e-mail: deposit@ccdc.cam.ac.uk.

## 9. Acknowledgements

A. B. and M. M. gratefully acknowledge the Université de Strasbourg and CNRS for financial support. The International Centre for Frontier Research in Chemistry (icFRC), and the Labex CSC (ANR-10-LABX-0026 CSC) within the Investissement d'Avenir program ANR-10-IDEX-0002-02 is also acknowledged for funding the PhD fellowship of A. B. M. M. kindly acknowledges the French Agence Nationale de Recherche (ANR) for the grant ANR-18-CE06-0007-01. The Institut Carnot MICA is kindly acknowledged for funding the exploratory project "Pt4Poly" and the scholarship to Z.A.

## 10. References

[1] (a) H. Takeda, K. Koike, T. Marimoto, H. Inumaru, O Ishitani, *Adv. Inorg. Chem.*, **2011**, *63*, 137; (b) R. A. Kirgan, B. P. Sullivan, D. P. Rillema, *Top. Curr. Chem.*, **2007**, *281*, 45; (c) A. Vlcek, Jr., *Top. Organomet. Chem.*, **2010**, *29*, 73; (d) M. Panigati, M. Mauro, D. Donghi, P. Mercandelli, P. Mussini, L. De Cola, G. D'Alfonso, *Coord. Chem. Rev.*, **2012**, *256*, 1621; (e) Z. Xue, Y. Dong, J. Ma. Z. Ou, *Polyhedron*, **2016**, *117*, 749.

[2] (a) M. Wrighton, D. L. Morse, *J. Am. Chem. Soc.*, **1974**, *96*, 998; (b) P. J. Giordano, S. M. Fredericks, M. S. Wrighton, D. L. Morse, *J. Am. Chem. Soc.*, **1978**, *100*, 2257; (c) P. J. Giordano, M. S. Wrighton, *J. Am. Chem. Soc.*, **1979**, *101*, 2888; (d) S. M. Fredericks, J. C. Luong, M. S. Wrighton, *J. Am. Chem. Soc.*, **1979**, *101*, 7415.]

[3] (a) L. Wallace, D. P. Rillema, *Inorg. Chem.*, **1993**, *32*, 3836; (b) L. Wallace, D. C. Jackman, D. P. Rillema, J. W. Merkert, *Inorg. Chem.*, **1995**, *34*, 5210.

[4] (a) L. Sacksteder, M. Lee, J. N. Demas, B. A. DeGraaf, *J. Am. Chem. Soc.*, **1993**, *115*, 8230; (b) L. Sacksteder, A. P. Zipp, E. A. Brown, J. Streich, J. N. Demas, B. A. DeGraff, *Inorg. Chem.*, **1990**, *29*, 4335.

[5] (a) J. Hawecker, J.-M. Lehn, R. Ziessel, *J. Chem. Soc., Chem. Commun.*, **1983**, 536; (b) J. Hawecker, J.-M. Lehn, R. Ziessel, *J. Chem. Soc., Chem. Commun.*, **1984**, 328; (c) B. P. Sullivan, C. M. Bolinger, D. Conrad, W. J. Vining, T. J. Meyer, *J. Chem. Soc., Chem. Commun.*, **1985**, 1414; (d) C. Kefalidi, E. Koutsouri, L. Marchiò, A. Zarkadoulas, S. Efstathiadou, C. A. Mitsopoulou, *Polyhedron*, **2016**, *110*, 157.

[6] (a) A. J. Amoroso, M. P. Coogan, J. E. Dunne, V. Fernández-Moreira, J. B. Hess, A. J. Hayes, D. Lloyd, C. Millet, S. J. A. Pope, C. Williams, *Chem. Commun.*, **2007**, 3066; (b) A. J. Amoroso, R. J. Arthur, M. P. Coogan, J. B. court, V. Fernández-Moreira, A. J. Hayes, D. Lloyd, C. Millet, S. J. A. Pope, *New J. Chem.*, **2008**, *32*, 1097.

[7] (a) G.-W. Zhao, J.-H. Zhao, Y.-X. Hu, D.-Y. Zhang, X. Li, *Synth. Met.*, **2016**, **212**, 131 and refs therein; (b) X. Li, H.-J. Chi, G.-H. Lu, G.-Y. Xiao, Y. Dong, D.-Y. Zhang, Z.-Q. Zhang, Z.-Z. Hu, *Org. Electr.*, **2012**, *13*, 3138.

[8] (a) D. Donghi, G. D'Alfonso, M. Mauro, M. Panigati, P. Mercandelli, A. Sironi, P. Mussini, L. D'Alfonso, *Inorg. Chem.*, **2008**, *47*, 4243; (b) M. Mauro, E. Quartapelle Procopio, C.-H. Chien, D. Donghi, M. Panigati, P. Mercandelli, P. Mussini, G. D'Alfonso, L. De Cola, *Adv. Funct. Mater.*, **2009**, *19*, 2607; (c) M. Mauro, C.-H. Yang, C.-Y. Shin, M. Panigati, C.-H. Chang, G. D'Alfonso, L. De Cola, *Adv. Mater.*, **2012**, *24*, 2054.

[9] (a) M. N. Hopkinson, C. Richter, M. Schedler, F. Glorius, *Nature*, **2014**, *510*, 485; (b) G. Bertrand, *J. Organomet. Chem.*, **2005**, *690*, 5397; (c) R. H. Crabtree, *Coord. Chem. Rev.*, **2007**, *251*, 595; (d) F. Glorius, *Top. Organomet. Chem.*, **2007**, *21*, 47; (e) S. P. Nolan, in *N-Heterocyclic Carbenes in Synthesis*; Wiley-VCH: Weinheim, Germany, **2006**; (f) W. A. Herrmann, C. Köcher, *Angew. Chem. Int. Ed. Engl.*, **1997**, *36*, 2162; (g) V. César, S. Bellemin-Laponnaz, L. H. Gade, *Chem. Soc. Rev.*, **2004**, *33*, 619; (h) W. A. Herrmann, L. J. Goossen, G. R. J. Artus, C. Köcher, *Chem. Rev.*, **2014**, *114*, 8747; (i) E. Peris, *Chem. Rev.*, **2018**, *118*, 9988; (l) F. Glorius (Ed.) in *N-Heterocyclic Carbenes in Transition Metal Catalysis*; Springer-Verlag: Berlin, **2007**; (m) J. C. Y. Lin, R. T. W. Huang, C. S. Lee, A. Bhattacharyya, W. S. Hwang, I. J. B. Lin, *Chem. Rev.*, **2009**, *109*, 3561; (n) S. Diez-Gonzalez, S. P. Nolan, *Coord. Chem. Rev.*, **2007**, *251*, 874; (o) H. V. Huynh, *Chem. Rev.*, **2018**, *118*, 9457.

[10] R. Visbal, M. C. Gimeno, *Chem. Soc. Rev.*, **2014**, *43*, 3551.

[11] Y. Chi, T.-K. Chang, P. Ganesan, P. Rajakannu, *Coord. Chem. Rev.*, **2017**, *346*, 91; A. Bonfiglio, M. Mauro, *Eur. J. Inorg. Chem.*, **2020**, 3427.

[12] (a) J. Soellner, M. Tenne, G. Wagenblast, T. Strassner, *Chem. Eur. J.*, **2016**, *22*, 9914; (b) A. Tronnier, U. Heinemeyer, S. Metz, G. Wagenblast, I. Muenster, T. Strassner, *J. Mater. Chem. C*, **2015**, *3*, 1680; (d) Y. Unger, D. Meyer, T. Strassner, *Dalton Trans.*, **2010**, *39*, 4295.

[13] Y. Chen, G. Cheng, L. Li, D. P. Shelar, W. Lu, C.-M. Che, *Chem. Sci.*, **2014**, *5*, 1348.

[14] (a) R. Hamze, J. L. Peltier, D. Sylvinson M. R., M. Jung, J. Cardenas, R. Haiges, M. Soleilhavoup, R. Jazzar, P. I. Djurovich, G. Bertrand, M. E. Thompson, *Science*, **2019**, *363*, 601; (b) S. Shi, M. C. Jung, C. Coburn, A. Tadle, D. Sylvinson M. R., P. I. Djurovich, S. R. Forrest, M. E. Thompson, *J. Am. Chem. Soc.*, **2019**, *141*, 3576; (c) M. Gernert, L.s Balles-Wolf, F. Kerner, U. Müller, A. Schmiedel, M. Holzapfel, C. M. Marian, J. Pflaum, C. Lambert, A. Steffen, *J. Am. Chem. Soc.*, **2020**, *142*, 8897; (d) M. Gernert, U. Müller, M. Haehnel, J. Pflaum, A. Steffen, *Chem. Eur. J.*, **2017**, *23*, 2206.

[15] W.-M. Xue, M. C.-W. Chan, Z.-M. Su, K.-K. Cheung, S.-T. Liu, C.-M. Che, *Organometallics*, **1998**, *17*, 1622.

[16] L. A. Casson, S. Muzzioli, P. Raiteri, B. W. Skelton, S. Stagni and M. Massi, *Dalton Trans.*, **2011**, *40*, 11960.

[17] (a) J. G. Vaughan, B. L. Reid, S. Ramchandani, P. J. Wright, S. Muzzioli, B. W. Skelton, P. Raiteri, D. H. Brown, S. Stagni, M. Massi, *Dalton Trans.*, **2013**, *42*, 14100; (b) J. G. Vaughan, B. L. Reid, P. J. Wright, S. Ramchandani, B. W. Skelton, P. Raiteri, S. Muzzioli, D. H. Brown, S. Stagni, M. Massi, *Inorg. Chem.*, **2014**, *53*, 3629; (c) P. V. Simpson, B. W. Skelton, P. Raiteri, M. Massi, *New J. Chem.*, **2016**, *40*, 5797.

[18] M. J. Stout, B. W. Skelton, A. N. Sobolev, P. Raiteri, M. Massi, P. V. Simpson, *Organometallics*, **2020**, *39*, 3202.

[19] (a) X.-W. Li, H.-Y. Li, G.-F. Wang, F. Chen, Y.-Z. Li, X.-T. Chen, Y.-X. Zheng, Z.-L. Xue, *Organometallics*, **2012**, *31*, 3829; (b) G.-F. Wang, Y.-Z. Liu, X.-T. Chen, Y.-X. Zheng, Z.-L. Xue, *Inorg. Chim. Acta*, **2013**, *394*, 488.

[20] A. Bonfiglio, K. Magra, C. Cebrián, F. Polo, P. C. Gros, P. Mercandelli, M. Mauro, *Dalton Trans.*, **2020**, *49*, 3102.

[21] A. J. Bard, L. R. Faulkner. *Electrochemical Methods: Fundamentals and Applications*, 2nd Ed., **2000**, Wiley.

[22] (a) N. J. Lundin, A. G. Blackman, K. C. Gordon, D. L. Officer, *Angew. Chem. Int. Ed.*, **2006**, *45*, 2582; (b) H. Hori, K. Koike, M. Ishizuka, K. Takeuchi, T. Ibusuki, O. Ishitani, *J. Organomet. Chem.*, **1997**, *530*, 169.

[23] "M86-EXX229V1 APEX3 User Manual", Bruker AXS Inc., Madison, USA, **2016**.

[24] G. M. Sheldrick, *Acta Cryst.* **2015**, A71, 3.

[25] G. M. Sheldrick, *Acta Cryst.* **2015**, C71, 3.

[26] G. A. Crosby, J. N. C. Demas, *J. Am. Chem. Soc.*, **1970**, *92*, 7262;

[27] I. Ishida, S. Tobita, Y. Hasegawa, R. Katoh, K. Nozaki, *Coord. Chem. Rev.*, **2010**, *254*, 2449.

[28] S. Antonello, M. Musumeci, D. D. M. Wayner, F. Maran, *J. Am. Chem. Soc.*, 1997, **119**, 9541.

[29] A. B. Meneses, S. Antonello, M. C. Arévalo, F. Maran, *Electroanalysis*, 2006, **18**, 363.

[30] Called PBE1PBE in Gaussian. (a) C. Adamo , V. Barone, *J. Chem. Phys.*, **1999**, *111*, 6158; (b) J. P. Perdew, K. Burke, M. Ernzerhof, *Phys. Rev. Lett.*, **1996**, *77*, 3865; (c) J. P. Perdew, K. Burke, M. Ernzerhof, *Phys. Rev. Lett.*, **1997**, *78*, 1396.

[31] (a) G. Scalmani, M. J. Frisch, B. Mennucci, J. Tomasi, R. Cammi, V. Barone, *J. Chem. Phys.*, **2006**, *124*, 094107; (b) G. Scalmani, M. J. Frisch, *J. Chem. Phys.*, **2010**, *132*, 114110.

[32] V. Barone, J. Bloino, M. Biczysko, F. Santoro, *J. Chem. Theory Comput.*, **2009**, *5*, 540.

[33] Gaussian 16 (revision A.03), Gaussian Inc., Wallingford, CT, **2016**.